Learning long temporal sequences in spiking networks by multiplexing neural oscillations

Philippe Vincent-Lamarre[1], Matias Calderini[1], and Jean-Philippe Thivierge[1]

[1] School of Psychology and Center for Neural Dynamics, University of Ottawa, Ottawa, Ontario, Canada

This manuscript was compiled on September 11, 2019

Many cognitive and behavioral tasks - such as interval timing, spatial navigation, motor control and speech - require the execution of precisely-timed sequences of neural activation that cannot be fully explained by a succession of external stimuli. We use a reservoir computing framework to explain how such neural sequences can be generated and employed in temporal tasks. We propose a general solution for recurrent neural networks to autonomously produce rich patterns of activity by providing a multi-periodic oscillatory signal as input. We show that the model accurately learns a variety of tasks, including speech generation, motor control and spatial navigation. Further, the model performs temporal rescaling of natural spoken words and exhibits sequential neural activity commonly found in experimental data involving temporal processing. In the context of spatial navigation, the model learns and replays compressed sequences of place cells and captures features of neural activity such as the emergence of ripples and theta phase precession. Together, our findings suggest that combining oscillatory neuronal inputs with different frequencies provides a key mechanism to generate precisely timed sequences of activity in recurrent circuits of the brain.

Reservoir computing | Neural oscillations | Temporal processing | Balanced networks

1. Introduction

Virtually every aspect of sensory, cognitive and motor processing in biological organisms involves operations unfolding in time (1). In the brain, neuronal circuits must represent time on a variety of scales, from milliseconds to minutes and longer circadian rhythms (2). Despite increasingly sophisticated models of brain activity, time representation remains a challenging problem in computational modelling (3, 4).

Recurrent neural networks offer a promising avenue to detect and produce precisely timed sequences of activity (5). However, it is challenging to train these networks due to their complexity (6), particularly when operating in a chaotic regime associated with biological neural networks (7, 8).

One avenue to address this issue is with the use of reservoir computing (RC) (9, 10). Under this framework, a recurrent network (the reservoir) projects onto a read-out layer whose synaptic weights are adjusted to produce a desired response. However, while RC can capture some behavioral and cognitive processes (11–13), it often relies on biologically implausible mechanisms (14). Further, current RC implementations offer little insight to understand how the brain generates activity that does not follow a strict rhythmic pattern (1, 5). That is because RC models are either restricted to learning periodic functions, or require an aperiodic input to generate an aperiodic output, thus leaving the neural origins of aperiodic activity unresolved (5). A solution to this problem is to train the recurrent connections of the reservoir to stabilize innate patterns of activity (12), but this approach is more computationally expensive and is sensitive to structural perturbations (15).

To address these limitations, we propose a biologically plausible spiking recurrent model that receives multiple independent sources of neural oscillations as input. The combination of oscillators with different periods creates a multi-periodic code that serves as a time-varying input that can largely exceed the period of any of its individual components. We show that this input can be generated endogenously by distinct subnetworks, alleviating the need to train recurrent connections of the reservoir to generate long segments of aperiodic activity. Further, no feedback from the output units to the reservoir was required during training (11, 16). Thus, multiplexing a set of oscillators into a reservoir network provides an efficient and neurophysiologically grounded means of controlling a recurrent circuit (15). Analogous mechanisms have been hypothesized in other contexts including grid cell representations (17) and interval timing (18, 19).

This paper is structured as follows. First, we describe a simplified scenario where a reservoir network that receives a collection of input oscillations learns to reproduce an arbitrary time-evolving signal. Second, we extend the model to show how oscillations can be generated intrinsically by oscillatory networks that can be either embedded or external to the reservoir. Third, we show that a network can learn several tasks in parallel by "tagging" each task to a particular phase configuration of the oscillatory inputs. Fourth, we show that the activity of the reservoir network captures temporal rescaling and selectivity, two features of neural activity reported during behavioral tasks. Fifth, we train the model to reproduce natural speech at different speeds when cued by input oscillations. Finally, we employ a variant of the model to capture hippocampal activity during spatial navigation. Together, results highlight a novel role for neural oscillations in regulating temporal processing within recurrent networks of the brain.

2. Results

A. A reservoir network driven by oscillations. We began with a basic implementation of our model where artificial oscillations served as input to a reservoir network (Fig. 1a) – in a later section, we will describe a more realistic version where recurrent networks generate these oscillations intrinsically. In this simplified model, two input nodes, but potentially more (Fig. S1),

generate sinusoidal functions of different frequencies. These input nodes project onto a reservoir composed of a recurrent spiking neural network. This network is a conductance-based leaky integrate-and-fire (LIF) model (20) with balanced excitation and inhibition (7). Every cell in the network is either strictly excitatory or inhibitory, thus respecting Dale's principle.

The combination of N_{inp} input oscillators will generate a sequence of unique N_{inp}-dimensional vectors where the sequence lasts as long as the least common multiple of the inputs' individual periods (15). For instance, two sine waves with periods of 200 ms and 250 ms would create a multi-periodic input with a period lasting 1,000 ms. This effect can be viewed as a two-dimensional state-space where each axis is an individual sine wave (Fig. 1b). Thus, multiplexed oscillations provide the network with inputs whose timescale largely exceeds that of individual units.

When a reservoir network ($N_{res} = 2,000$) was injected with oscillations, excitatory and inhibitory populations modulated their activity over time, while the average input currents to individual neurons remained balanced (Fig. 1c, top panel). To illustrate the benefits of oscillatory inputs on a reservoir, we designed a simple task where a network was trained to reproduce a target function consisting of a time-varying signal generated from low-pass filtered noise (Fig. 1c, bottom panel). Simulations were split into a training and a testing phase. During the training phase, the network received a combination of two oscillatory inputs at 4 and 5 Hz. Synaptic weights from the reservoir to the read-out were adjusted using the regularized least-squares learning algorithm (21) adapted to spiking units (13). During the testing phase, synaptic weights were frozen and the network's performance was assessed by computing the Pearson correlation between the target function and the network's output. This correlation increased to 0.9 within the first 10 training epochs and remained stable thereafter (Fig. 1d). By comparison, the output of a similar network with no oscillatory inputs remained uncorrelated to the target function. Thus, oscillatory inputs provided rich and reliable dynamics that enabled the reservoir to produce a target function that evolved over time in a precise manner.

Next, we investigated the resilience of the network to structural perturbations where a number of individual neurons from the reservoir were "clamped" (i.e., held at resting potential) after training (15). We trained a network for 10 epochs, then froze the weights and tested its performance on producing the target output. We then gradually clamped an increasing proportion of neurons from the reservoir. The network's performance decreased gradually as the percentage of clamped units increased (Fig. 1e). Remarkably, the network produced an output that correlated strongly with the target function (correlation of 0.7) even when 10% of neurons were clamped. Further exploration of the model shows a wide range of parameters that yield high performances (Fig. S1). Oscillatory inputs thus enabled reservoir networks to produce precise and repeatable patterns of activity under a wide range of modeling conditions. Next, we improved upon this simple model by developing a more biologically-inspired network that generated oscillations intrinsically.

B. Endogenously generated oscillatory activity. While our results thus far have shown the benefits of input oscillations when training a reservoir model, we did not consider their neural origins. To address this issue, we developed a model that replaces this artificial input with activity generated by an "oscillator" spiking network acting as a central pattern generator (22).

To do so, we took advantage of computational results showing that sparsely connected networks can transition from an asynchronous to a periodic synchronous regime in response to a step current (23–25), thus capturing *in vivo* activity (26) (see Methods) (Fig. 2a). The periodicity of the synchronous events could therefore potentially be used to biologically capture the effects of artificially generated sine waves.

In simulations, we found that this transition was robust to both synaptic noise and neuronal clamping (Fig. S2). Further, the frequency of synchronized events could be modulated by adjusting the strength of the step current injected in the network, with stronger external inputs leading to a higher frequency of events (Fig. S2). Thus, oscillator networks provide a natural neural substrate for input oscillations into a recurrent network.

From there, we formed a model where three oscillator networks fed their activity to a reservoir network (Fig. 2b). These oscillator networks had the same internal parameters except for the inhibitory decay time constants of their recurrent synapses ($\tau_{in} = 70$, 100 and 130 ms for each network) thus yielding different oscillatory frequencies (Figs. S3,S4). In order to transition from an asynchronous to a synchronous state, the excitatory neurons of the oscillator networks received a step current.

The full connectivity matrix of this large model is depicted in Fig. 2c. As shown, the oscillator networks send sparse projections (with a probability of 0.3 between pairs of units) to the reservoir units. Only the excitatory neurons of the reservoir network project to the readout units. Only weak feedback from the reservoir to the oscillators was included - in supplementary simulations, we found that strong feedback projections desynchronized the oscillator networks (Figs. S2,S5).

A sample of the full model's activity is shown in Fig. 2e. Both the oscillator and the reservoir networks showed asynchronous activity until a step current was injected into the excitatory units of the oscillator networks. In response to this step current, both oscillator and reservoir networks transitioned to a synchronous regime. The model reverted back to an asynchronous regime once the step current was turned off.

To illustrate the behavior of this model, we devised a "cued" task similar to the one described above, where the goal was to reproduce a random time-varying signal. When learning this signal, however, the oscillator networks received a cue ("Input 1") consisting of a combination of excitatory step current and transient inhibitory input (Fig. 2d) that alters the relative phase of the input oscillators, but not their frequency. Following 20 epochs of training, we switched to a testing phase and showed that

[1]Philippe Vincent-Lamarre. E-mail: pvinc058@uottawa.ca
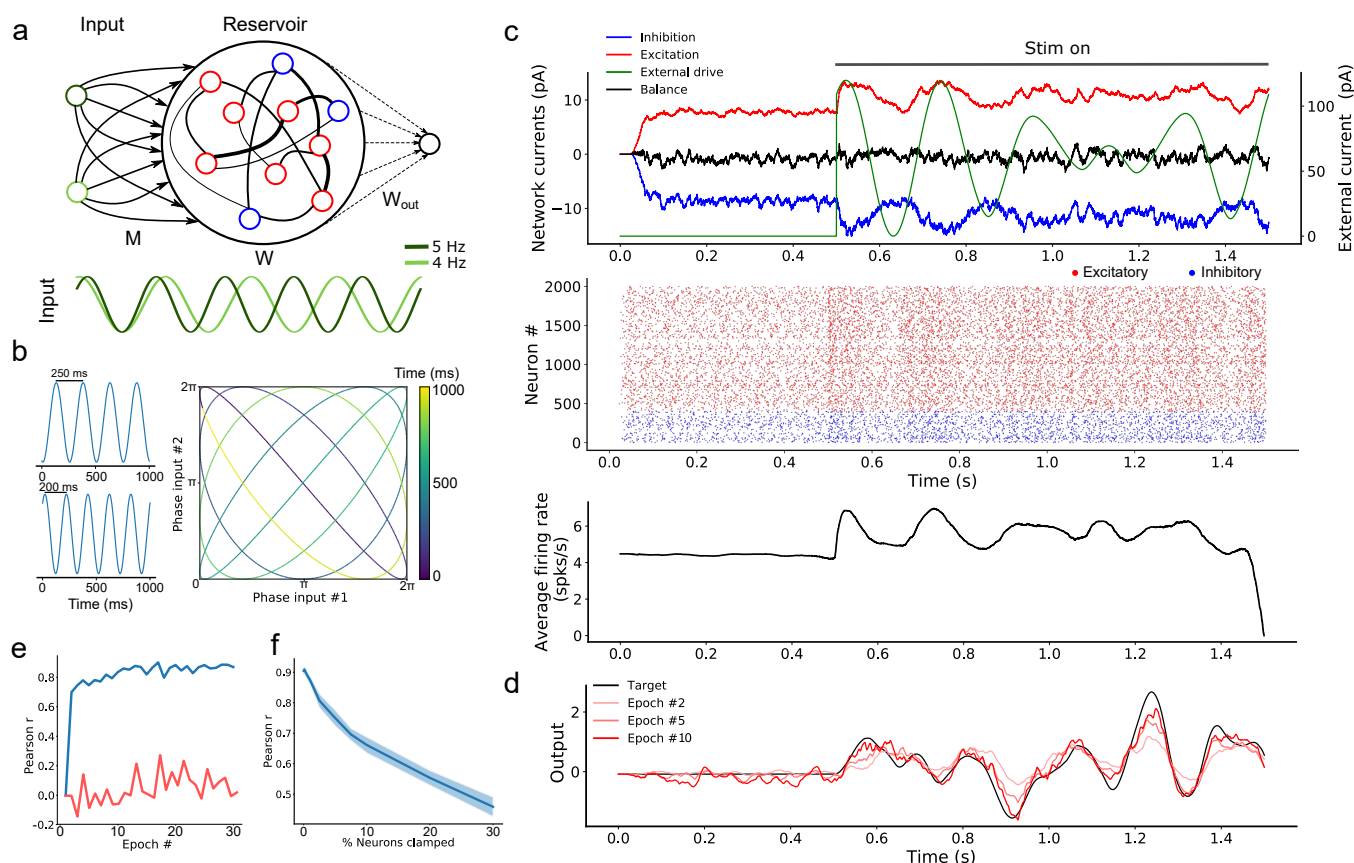
Vincent-Lamarre *et al.*

Fig. 1. Oscillation driven spiking recurrent network as a reservoir computing model. **a** Schematic of the model's architecture. This implementation has two input units that inject sine-waves in a subset of the reservoir's neurons. M denotes the connections from the input units to the reservoir neurons. W denotes the recurrent connectivity matrix of the reservoir. W_{out} denotes the trainable connections from the excitatory reservoir neurons to the readout unit. **b** Example showing how two sine waves of different frequencies can be combined to generate a two-dimensional function with a period longer than either sine wave. **c** Sample average current per neuron, raster and average instantaneous firing rate respectively. The external drive is only delivered to a subset of reservoir units (p_{inp} = 0.3) for each input unit. **d** Output of the readout unit during testing trials (learning rule turned off) interleaved during training. **e** Pearson correlation between the output of the network and the target function as a function of the number of training epochs when driven with (blue) and without (red) multi-periodic input. **f** Pearson correlation between the output and the target function as neurons of the reservoir are clamped.

the model closely matched the target signal (Fig. 2f). Crucially, this behavior of the model was specific to the cue provided during training: when a different, novel cue (shaped by inhibitory transients) was presented to the network ("Input 2"), an different output was produced (Fig. 2f).

In sum, the model was able to learn a complex time-varying signal by harnessing internally-generated oscillations that controlled the ongoing activity of a reservoir network. In the following section, we aimed to further explore the computational capacity of the model by training a reservoir on multiple tasks in parallel.

C. An artificial network that learns to multitask. To explore the ability of the model to learn two tasks concurrently, we reverted to our initial model with artificial oscillations, allowing for a more principled control of the input injected to the reservoir network. The oscillatory input consisted of three sine waves of different frequencies (Fig. 3a) (more inputs lead to richer dynamics, Fig. S1) .

We trained this model on two different motor control tasks that required the network to combine the output of two readout units in order to draw either a circle or a star in two dimensions. Here, each of the outputs corresponded to x- and y-coordinates, respectively. The phase of the oscillations ("Input 1" vs. "Input 2") were individually paired with only one of the two tasks in alternation (Fig. 3a).

We employed a principal component analysis (PCA) to visualize the activity of the reservoir before and during training (Fig. 3b). Before injecting the oscillatory inputs, the network generated spontaneous activity that occupied a limited portion of the state space (Fig. 3b, circle). During training, the oscillatory inputs were turned on, resulting in different trajectories depending on the relative phase of the oscillations. The network thus displayed a distinct pattern of activity for each of the two tasks.

Viewed in two dimensions, the outputs of the network rapidly converged to a circle and a star that corresponded to each of the two target shapes when given each respective input separately (Fig. 3c). These shapes were specific to the particular phase of the oscillatory input – in a condition where we presented a randomly-chosen phase configuration to the network, the output did not match either of the trained patterns (Fig. 3c).

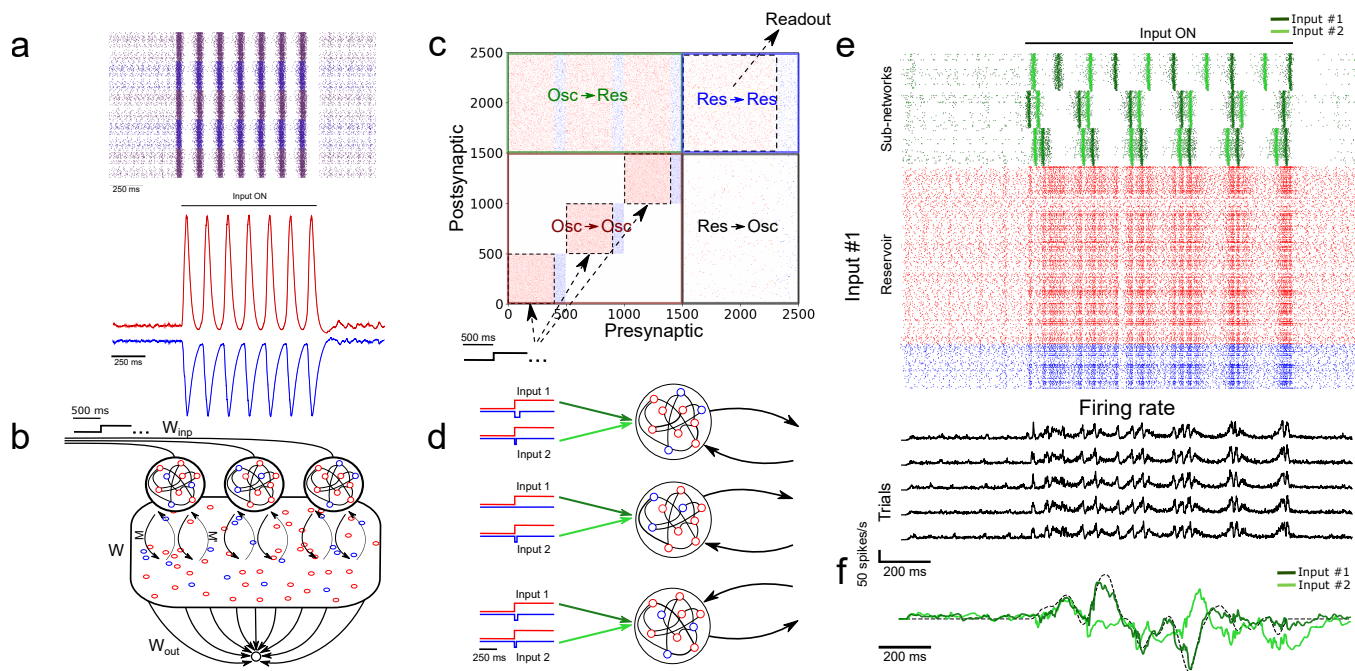Finally, we tested the ability of the model to learn a number of target signals varying in duration and frequency. We

Fig. 2. Reservoir driven with intrinsically generated oscillations. **a** Top: Sample rasters from one network on five different trials. Bottom: Average and standard error of the excitatory (red) and inhibitory (blue) conductance of a stable network on 5 different trials. The network is asynchronous when the external drive is off, and becomes periodic when turned on. **b** Architecture of the augmented model. As in 1a, W and W_{out} denote the recurrent and readout connections, respectively. M is the connection matrix from the input to the reservoir, except that the input units are now replaced by networks of neurons. M' denotes the feedback connections from the reservoir to the oscillatory network. W_{inp} denotes the connections providing the tonic depolarization to the oscillatory networks. **c** Connectivity matrix of the model. The external drive is provided solely to the oscillatory networks that project to the reservoir network that in turn projects to the readout unit. **d** External inputs provided to the oscillatory networks with varied inhibitory transients associated with eac. **e** Top: Sample activity of the oscillatory networks (green) on two separate trials with different inputs, and the reservoir for one trial (input #1). Bottom: PSTH of the network's activity on five different trials with input #1. **f** Post-training output of the network, where input #1 was paired with the target, but input #2 was not.

generated a number of target functions consisting of filtered noise (as described previously), and varied their duration as well as the cut-off frequencies of band-pass filtering. The network performed optimally for tasks with relatively low frequency (<30 Hz) and shorter duration (<5 seconds), and had a decent performance for even longer targets (e.g, correlation of $r=0.5$ for a time of 7 seconds and a frequency below 30 Hz). (Fig. 3d).

In sum, the model was able to learn multiple tasks in parallel based on the phase configuration of the oscillatory inputs to the reservoir units. The range of target signals that could be learned was dependent upon their duration and frequency. The next section will investigate another aptitude of the network, where a target signal can be rescaled in time without further training.

D. Temporal rescaling of neuronal activity. A key aspect of many behavioral tasks based on temporal sequences is that once learned they can be performed faster or slower without additional training. For example, when a new word is learned, it can be spoken faster or slower without having to learn the different speeds separately.

We propose a straightforward mechanism to rescale a learned temporal sequence in the model. Because the activity of the model strongly depends upon the structure of its oscillatory inputs, we conjectured that the model may generate a slower or faster output by multiplying the period of the oscillatory inputs by a common factor. Biologically, such a factor might arise from afferent neural structures that modulate oscillatory activity (23). Due to the highly non-linear properties of the network, it is not trivial that rescaling the inputs would expand or compress its activity in a way that preserves key features of the output (27).

To test the above mechanism, we trained a reservoir network receiving sine wave inputs to produce a temporal sequence of low-pass filtered random activity. After the pair of input-target was trained for 10 epochs, we tested the network by injecting it with sine waves that were either compressed or expanded by a fixed factor relative to the original inputs (Fig. 4a). To evaluate the network's ability to faithfully replay the learned sequence, we computed the Pearson correlation between the output of the network (Fig. 4b) and a compressed or expanded version of the target signal.

Performance degraded gradually with inputs that were expanded or contracted in time relative to the target signal (i.e, as the rescaling factor moved further away from 1) (Fig. 4c). Further, performance degraded more slowly beyond a rescaling factor of 1.5, particularly when input noise was absent, suggesting some capacity of the network to expand the target signal in time (Fig. S6). This result offered a qualitative match to experimental findings (28) and the performance of the network was robust to the addition of random jitter in the phase of the input oscillations (Fig. S7).

In sum, rescaling the speed of the input oscillations by a common factor lead to a corresponding rescaling of the learned task, with compressed neural activity resulting in more error than expanded activity. The next section examines some of the
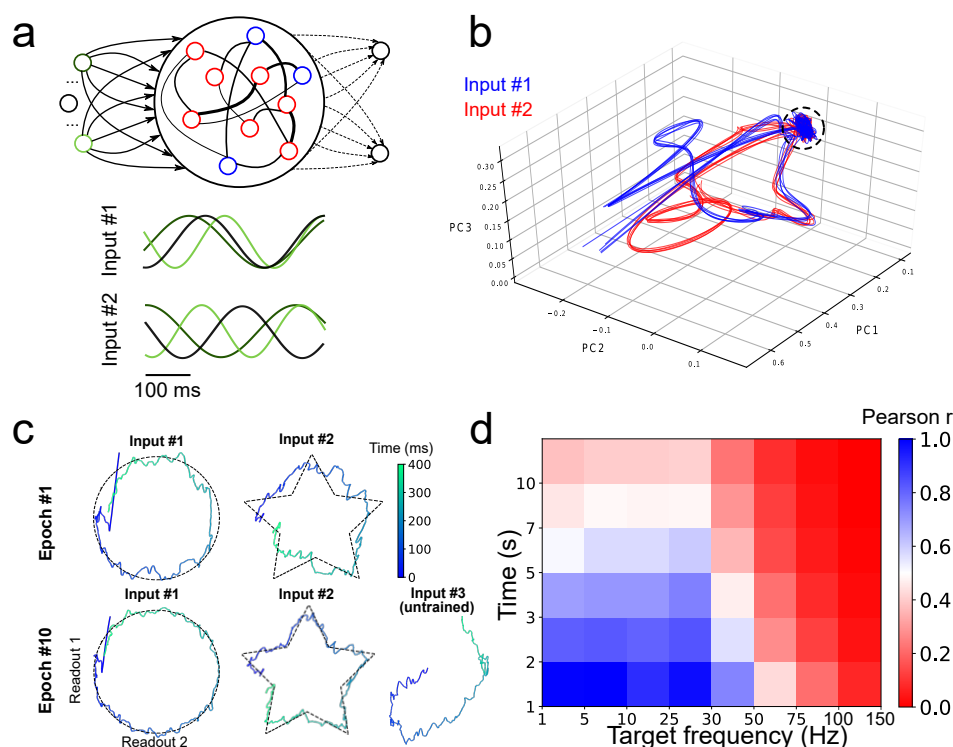
Vincent-Lamarre *et al.*

Fig. 3. Parallel training of multiple tasks. **a** Schematic of the model's architecture with an additional readout unit. An example of possible phase shifted inputs is shown at the bottom. **b** Trajectory of the reservoir on the first three components of a PCA. Without an external input, the network is spontaneously active and constrained in a subspace of the state-space (depicted by the circle). Upon injection of the input, the reservoir's activity is kicked into the trajectory related to the input. **c** Output of the two readout units after the first and tenth training epochs. **d** Heat map showing the performance of the model on tasks with different lengths and frequencies.

underlying features of activity in a reservoir network driven by oscillatory inputs.

E. Temporal selectivity of artificial neurons. A hallmark of temporal processing in brain circuits is that some subpopulations of neurons increase their firing rate at specific times during the execution of a timed task (29–31). To see whether this feature was present in the model, we injected similar oscillatory inputs as above (10 input units between 5 and 10 Hz for 1 second) for 30 trials. To match experimental analyses, we convoluted the firing rate of each neuron from the reservoir with a Gaussian kernel (s.d. = 20 ms), averaged their activity over all trials, and converted the resulting values to a z-score. To facilitate visualization, we then sorted these z-scores by the timing of their peak activity. We retained only the neurons that were active during the simulations (71%). Results showed a clear temporal selectivity whereby individual neurons increased their firing rate at a preferred time relative to the onset of each trial (Fig. 4d).

These "selectivity peaks" in neural activity were maintained in the same order when we expanded or contracted the input oscillations by a fixed factor (Fig. 4a), and sorted neurons based on the original input oscillations (Fig. 4d), thus capturing recent experimental results (30). To shed light on the ability of simulated neurons to exhibit temporal selectivity, we examined the timing of excitatory and inhibitory currents averaged across neurons of the reservoir. We then aligned these currents to the timing of selectivity peaks and found elevated activity around the time of trial-averaged peaks (Fig. 4e). Therefore, both the input E/I currents and the external inputs drive the activity of the neurons near their peak response, showing that an interaction between intrinsic and external sources drives the temporal selectivity of individual neurons.

In sum, neurons from the reservoir show sequential patterns of activity by leveraging a combination of external drive and recurrent connections within the network. Next, we examined the ability of the model to learn a naturalistic task of speech production.

F. Learning Natural Speech, Fast and Slow. In a series of simulations, we turned to a biologically and behaviorally relevant task of natural speech learning. This task is of particular relevance to temporal sequence learning given the precise yet flexible nature of speech production: once we learn to pronounce a word, it is straightforward to alter the speed at which this word is spoken without the need for further training. We thus designed a task where an artificial neural network must learn to utter spoken words in the English language and pronounce them slower or faster given the appropriate input, without retraining.

To train a network on this task, we began by extracting the waveform from an audio recording of the word "reservoir" and converting this waveform to a spectrogram (Fig. 5a). We then employed a compression algorithm to bin the full range of frequencies into 64 channels spanning a range from 300 Hz to 8 kHz (see Methods). Each of these channels were mapped onto an individual readout unit of the model. Synaptic weights of the reservoir to the readout were trained to reproduce the
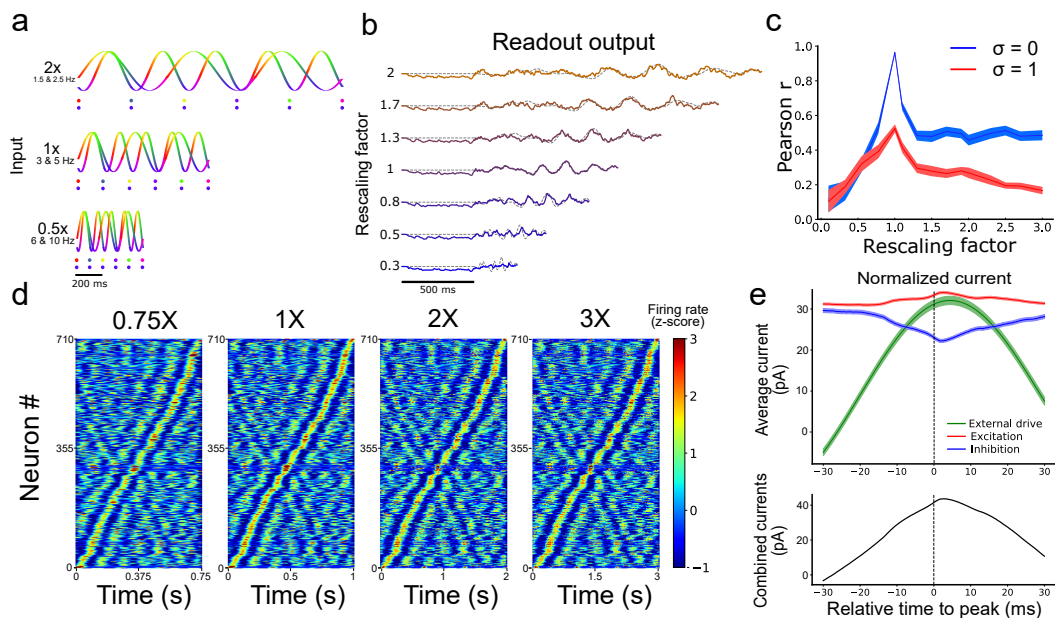
Fig. 4. Temporal rescaling of the network's activity. **a** Activity of two input units with different rescaling factors. Each phase is represented in a different color. The two dots shown for the different velocities are spaced at a constant proportion of the whole duration, and show that the phase alignment of the two oscillators is preserved across different rescaling factors. **b** Output of the network for different rescaling factors. The target is represented by the grey dashed line. **c** Pearson correlation between the output and the target function for different rescaling factors and different input noise variance (σ). **d** Spiking activity of the reservoir at 0.75X, 1X, 2X, and 3X sorted based on the peak of the activity at the original scaling (1X). **e** Average excitatory (red), inhibitory (blue), and external input (green) received by each cell aligned on their peak firing rate (at t = 0 ms). The combined inputs (black, external + excitation - inhibition) is represented at the bottom.

amplitude of the 64 channels over time. The output spectrogram obtained from the readout units was converted to an audio waveform and compared to the target waveform (see Movie S1).

Following training, the network was able to produce a waveform that closely matched the target word (Fig. 5a). To examine the ability of the network to utter the same word faster or slower, we employed the rescaling approach described earlier, where we multiplied the input oscillations by a constant factor (Fig. 4a).

Our model was able to produce both faster and slower speech than what it had learned (Fig. 5b). Scaling the outputs back to the original speed showed that the features of the spectrogram were well replicated (Fig. 5c). The correlation between the rescaled outputs and target signal decreased as a function of the rescaling factor (Fig. 5d), in a manner similar to the above results on synthetic signals (Fig. 4c).

Results thus suggest that multiplexing oscillatory inputs enabled a reservoir network to acquire and rescale temporal sequences obtained from natural speech. In the final section below, we employed our model to capture hippocampal activity during a well-studied task of spatial navigation.

G. Temporal sequence learning during spatial navigation. Thus far, we have modelled tasks where units downstream of the reservoir are learning continuous signals in time. In this section, we turned to a task of spatial navigation that required the model to learn a discrete sequence of neural activity.

A wealth of experiments shows that subpopulations of neurons become selectively active for specific task-related time intervals. A prime example is seen in hippocampal theta sequences (32) that emerge during spatial navigation in rodents, where individual place cells (33) increase their firing rate at a given location in space (place fields). During spatial navigation, the hippocampus shows oscillatory activity in the theta range (4-12 Hz), likely originating from both the medial septum (34)) and within hippocampus (35, 36) .

In a series of simulations, we examined how neurons in a reservoir network may benefit from theta oscillations to bind and replay such discrete place cells sequences. We designed a reservoir (associated with area CA1,(32)) that received inputs from multiple input oscillators (CA3, (37)) (Fig. 6a,b). We randomly selected 10 excitatory units within the reservoir and labelled them as "place cells". To simulate the response of place cells to an environmental input indicating the spatial location of the animal (38), we depolarized these cells by an oscillating input at 10 Hz for 600 ms with a specific onset that differed across neurons in order to capture their respective place fields (assuming a fixed spatiotemporal relation of 100 ms = 5 cm on a linear track). In this way, the sequential activation of place cells from the reservoir network mimicked the response of CA1 neurons to an animal walking along a linear track (Fig. 6c).

To capture the effect of theta oscillations on CA1 activity, all neurons from the reservoir were driven by a combination of multiple oscillating inputs where the frequency of each input was drawn from a uniform distribution in the range of 7-9 Hz. Connections from the input units and the place cells within the reservoir were modified by a synaptic plasticity rule (see Methods).
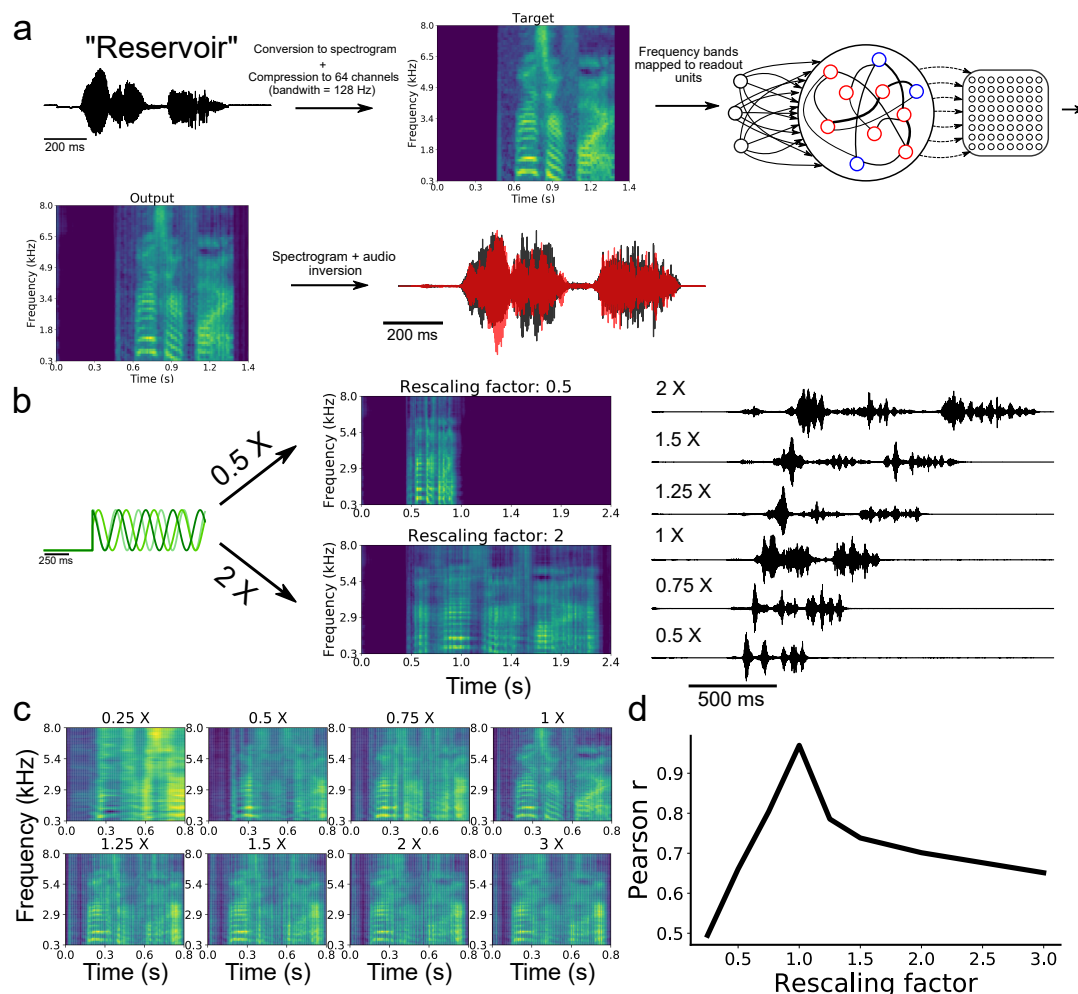
Fig. 5. Speech learning and production with temporal rescaling. **a** Workflow of the transformation and learning of the target audio sequence. **b** The input frequencies are either sped-up or slowed-down in order to induce temporal rescaling of the speed of execution of the task. **c** The rescaled output spectrograms are scaled back to the original speed in order to compare them to the target spectrogram. **d** Average correlation between the output and target of all channels of the spectrograms for the different rescaling factors.

As expected from the input oscillators, mean population activity of the reservoir network exhibited prominent theta activity (Fig. 6d). To assess the baseline performance of the model, we ran an initial simulation with oscillatory inputs but no synaptic plasticity or place fields (i.e., no environmental inputs to the place cells). All place cells of the model remained silent (Fig. 6g). Next, we ran a training phase simulating a single lap of the virtual track lasting 5 seconds, where place cells received oscillatory inputs (CA3) as well as a depolarizing oscillation (10 Hz) whenever the cell entered its place field. During this lap, individual place cells entered their respective field only once. We assessed the performance of the model during a testing phase where both synaptic plasticity and depolarizing oscillations were turned off. During the testing phase, place cells yielded a clear sequence of activation that matched the firing pattern generated during training (Fig. 6g). Thus, place cell activity was linked to the phase of the oscillatory inputs after a single lap of exploration.

Going further, we explored two key aspects of place cell activity in the reservoir that are reported in hippocampus, namely phase precession and rapid replay. During phase precession, the phase of firing of place cells exhibits a lag that increases with every consecutive cycle of the theta oscillation (32, 39). We examined this effect in the model by extracting the instantaneous phase of firing relative to the global firing rate filtered between 4-12 Hz. The activity of individual place cells from the reservoir relative to theta activity exhibited an increasing phase lag characteristic of phase precession (Fig. 6e,f).

A second feature of hippocampal activity is the rapid replay of place cells during rest and sleep in a sequence that mirrors their order of activation during navigation (40). This replay can arise in either a forward or reverse order from the original sequence of activation (41). We compressed (factor of 0.15) the CA3 theta oscillations injected in the reservoir during training, resulting in rapid (50-55 Hz) bursts of activity (Fig. 6h). These fast oscillations mimicked the sharp-wave ripples that accompany hippocampal replay (40). In response to these ripples, place cells of the reservoir exhibited a pattern of response that conserved the order of activation observed during training (Fig. 6h). Further, a reverse replay was obtained by inverting the ripples (that is, reversing the order of the compressed sequence) presented to the reservoir (Fig. 6h).

In sum, oscillatory inputs allowed individual neurons of the model to respond selectively to external inputs in a way that

228   captured the sequential activation and replay of hippocampal place cells during a task of spatial navigation.
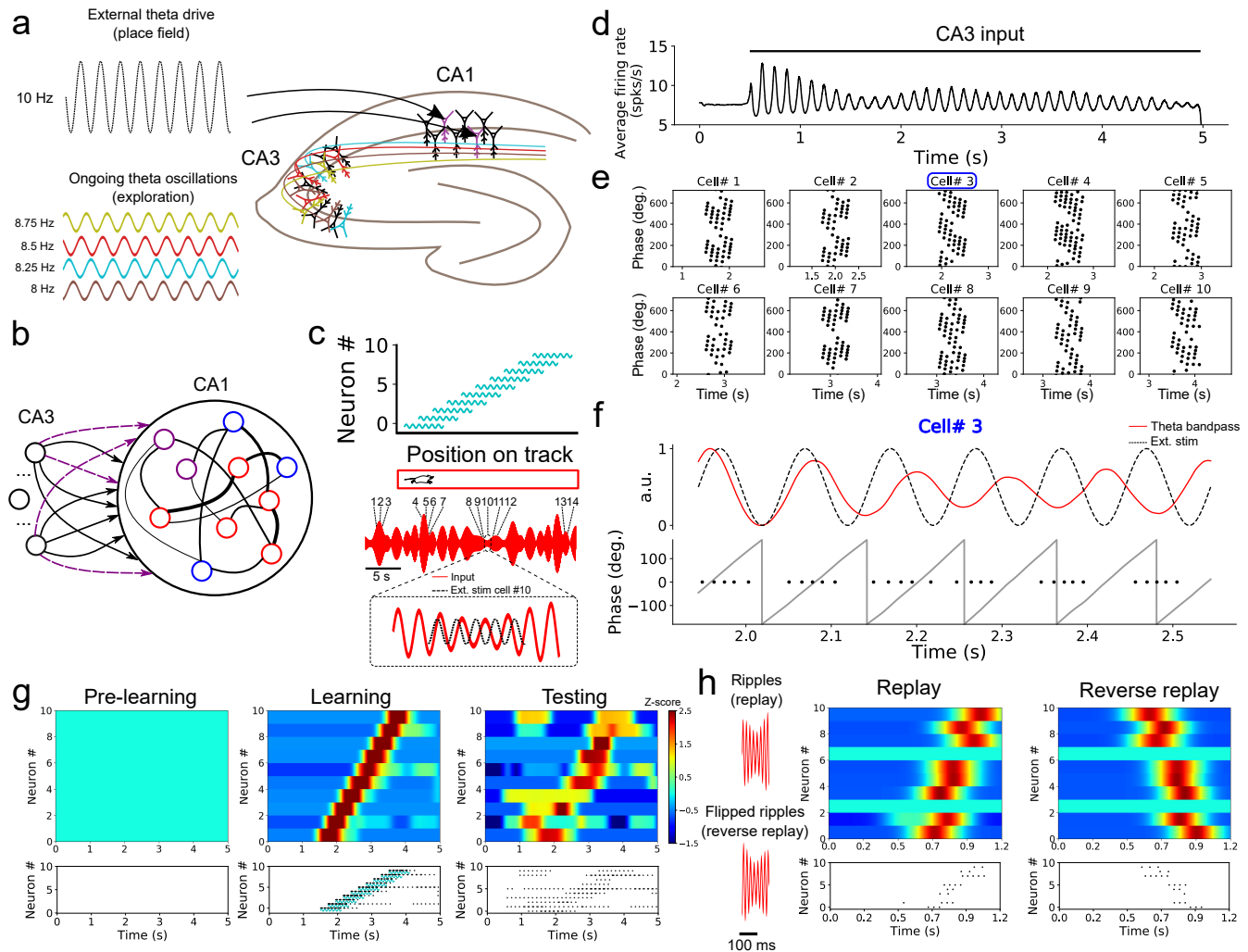

Fig. 6. Formation of place cell sequences and replay. **a** Subpopulations of CA3 cells oscillating in the theta range and projecting to CA1. CA1 place cells are driven by a slightly faster oscillating input upon entering their place field. **b** RC implementation of the phenomenological model. The input layer is composed of oscillatory units (CA3) and CA1 is modelled by a reservoir where 10 excitatory units (purple) are randomly selected as place cells. The connections from the input to the place cells are subject to training. **c** Top: Each of the 10 reservoir place cells were driven by a depolarizing oscillating input in a temporal sequence analogous to a mouse moving along a linear track. Bottom: Resulting theta frequency of the combined oscillations (red). Each number shows a place cell activated at a given time along the ongoing theta input. The multi-periodic input from CA3 guarantees that each place cell is activated with a unique combination of the input, following the sequence in which the cell is active. **d** Multiplexing CA3 inputs generates a visible theta oscillation in the CA1 reservoir. **e** Spike times of the ten place cells in relation to the phase of the population theta activity. Each dot represents a spike at a certain time/position. Each cell shows a shift towards earlier theta phase as the animal moves along its place fields. **f** Activity of cell #3 upon entering its place field. Top: theta band-passed activity of the reservoir (red) and place field related input (dashed black). Bottom: phase of the theta oscillation (grey) and spike times. **g** Top shows a heatmap of the place cell activity and bottom shows the spike raster during each phase of training. Before training: All place cells are silent. During training: place cells are depolarized upon entering their place field. After training: a similar sequence is evoked without the external stimulation used during training. **h** Rescaling the input (factor of X0.15) leads to a high-frequency input reminiscent of ripples. A compressed version of the sequence learned in **g** is evoked, and a reversed sequence is evoked when a reverse "ripple" is injected in the reservoir.

229 ## 3. Discussion

230   **A. Summary of results.** Taken together, our results suggest that large recurrent networks can benefit from autonomously
231 generated oscillatory inputs in order to learn a wide variety of artificial and naturalistic signals, and exhibit features of neural
232 activity that closely resemble neurophysiological experiments.

233   One series of simulations trained the model to replicate simple shapes in 2D coordinates. Based upon the structure of its
234 oscillatory inputs, the model flexibly switched between two shapes, thus showing a simple yet clear example of multitasking
235 with a recurrent network.

236   When we modulated the period of input oscillations delivered to neurons of the reservoir, the model was able to produce an
237 output that was faithful to the target signal, but sped up or slowed down by a constant factor (28, 30). Oscillations served to
238 train a recurrent network that reproduced natural speech and generated both slower and faster utterances of natural words

with no additional training. Using further refinements of the model, we employed this principle of oscillation-driven network to capture the fast replay of place cells during a task of spatial navigation.

Below we discuss the biological implications of our model as well as its applications and limitations.

B. Biological relevance and predictions of the model. Despite some fundamental limitations common to most computational models of brain activity, our approach was designed with several key features of living neuronal networks, including spiking neurons, Dale's principle, balanced excitation/inhibition, a heterogeneity of neuronal and synaptic parameters, propagation delays, and conductance-based synapses (7, 11, 42).

Further, and most central to this work, our model included neural oscillations along a range of frequencies that closely matched those reported in electrophysiological studies (26, 43). Although there is an abundance of potential roles for neural oscillations in neuronal processing, much of their function remain unknown (44). Here, we proposed that multiple heterogeneous oscillations may be combined to generate an input whose duration greatly exceeds the time-course of any individual oscillation. In turn, this multiplexed input allows a large recurrent network operating in the chaotic regime to generate repeatable and stable patterns of activity that can be read out by downstream units.

It is well established that central pattern generators in lower brain regions such as the brain stem and the spinal cord are heavily involved in the generation of rhythmic movements that match the period of simpler motor actions (e.g. walking or swimming) (45). From an evolutionary perspective, it is compelling that higher brain centers would recycle the same mechanisms (43) to generate more complex and non-repetitive actions (46, 47). In this vein, (47) showed that both periodic and quasi-periodic activity underlie a non-periodic motor task of reaching. Our model provides a framework to explain how such activity can be exploited by living neuronal networks to produce rich dynamics whose goal is to execute autonomous aperiodic tasks.

While our model shows that oscillatory networks can generate input oscillations that control the activity of a reservoir (Fig. 2), the biological identity of these oscillatory networks is largely circuit-dependent and may originate from either intrinsic or extrinsic sources. In the hippocampus, computational (35) and experimental (36) findings suggest an intrinsic source to theta oscillations. Specifically, studies raise the possible role of CA3 in forming a multi-periodic drive consisting of several interdependent theta generators that activate during spatial navigation (37).

Similarly, the neural origin of the tonic inputs controlling the activity of the oscillatory networks is not explicitly accounted for in our simulations. However, it is well established that populations of neurons can exhibit bistable activity with UP-states lasting for several seconds (48) that could provide the necessary input to drive the transition from asynchronous to synchronous activity in oscillatory networks.

Going beyond an *in silico* replication of neurophysiological findings, our model makes two empirically testable predictions. If one was to experimentally isolate the activity of the input oscillators, one could show that: (i) a key neural signature of a recurrent circuit driven by multi-periodic oscillations is the presence of inter-trial correlations between the phase of these oscillations; and (ii) the period of the input oscillators should appear faster or slower to match the rescaling factor of the network. This correspondence between the input oscillations and temporal rescaling is a generic mechanism behind the model's ability to perform a wide variety of tasks, from spatial navigation to speech production.

C. Related models. Our approach was inspired by predecessors in computational neuroscience. Multiplexing multiple oscillations as a way to generate long sequences of non-repeating inputs was first introduced by (18), with a model of interval timing relying on the coincident activation of multiple oscillators of different frequencies. This idea served as a basis for the striatal beat frequency model (19), where multiple cortical regions are hypothesized to project to the striatum which acts as a coincidence detector that encodes timing intervals. A similar mechanism was also suggested for the representation of space by grid cells in rodents (17). Grid cells have periodic activation curves spanning different spatial periods (49), and their activation may generate a combinatorial code employed by downstream regions to precisely encode the location of the animal in space (17).

Other studies have suggested that phase precession during spatial navigation could originate from a dual oscillator process (39, 50). Along this line, a recent model of the hippocampus uses the interference between two oscillators to model the neural dynamics related to spatial navigation (51). Although this model shares similarities with ours, a fundamental difference is that our model uses the phase of combined oscillators to create a unique input at every time-step of a task, whereas their model relies on the beat of the combined frequencies. Additionally, in our model, increasing the frequency of input oscillations by a common factor leads to compressed sequences of activity. By comparison, in the model of (51), sequences are compressed by removing an extrinsic input oscillator. More experimental data will be needed to support either model.

D. Limitations and future directions. In our model, periodic activity was readily observable in the reservoir dynamics due to the input drive (e.g. Fig. 1c or Fig. 6d). However, the architecture of our model represents a simplification of biological networks where several intermediate stages of information processing occur between sensory input and behavioral output. Oscillatory activity resulting from a multi-periodic drive might occur in one, but not necessarily all stages of processing. Further work could examine this issue by developing a multi-layered network of reservoirs; such a hierarchical organization may have important computational benefits (52).

In the spatial navigation task, we ensured that the location of the animal was perfectly correlated with the time spent in the place field of each cell. This is, of course, an idealized scenario that does not account for free exploration and variable speed of navigation along a track. These factors would decorrelate the spatial location of the animal and the time elapsed in the place field. Hence, further work would benefit from a more ecologically-relevant version of the navigation task. This new

298 version of the task might aim to capture how the time spent in a given place field impacts the link between the activity of
299 place cells and theta oscillations (53) .
300 Finally, our task of speech production was restricted to learning a spectrogram of the target signal. This simplified task did
301 not account for the neural control of articulatory speech kinetics, likely involving the ventral sensory-motor cortex (54, 55).

302 **D.1. Applications.** Our modeling framework is poised to address a broad spectrum of applications in machine learning of natural
303 and artificial signals. With recent advances in reservoir computing (56) and its physical implementations (57), our approach
304 offers an alternative to using external arbitrary time-varying signals to control the dynamics of a recurrent network. Our model
305 may also be extended to neuromorphic hardware, where it may benefit chaotic networks employed in robotic motor control (58).
306 Finally, our model is, to our knowledge, the first to produce temporal rescaling of natural speech, with implications extending
307 to conversational agents, brain-computer interfaces, and speech synthesis.
308 Overall, our model offers a compelling theory for the role of neural oscillations in temporal processing. Support from
309 additional experimental evidence could impact our understanding of how brain circuits generate long sequences of activity that
310 shape both cognitive processing and behavior.

4. Methods

A. Integrate-and-fire networks.

A.1. Driven networks. Our network consists of leaky integrate-and-fire neurons, where $N_{res} = 1,000$ for the reservoir and
$N_{osc} = 500$ for each oscillatory network, by default. 80% of these neurons are selected to be excitatory while the remaining
20% are inhibitory. The membrane potential of all neurons is given by

$$C\frac{dV}{dt} = \frac{1}{R}(E_L - V) + g_{ex}(E_{ex} - V) + g_{in}(E_{in} - V) + I_{tonic} + I_{inp} \tag{1}$$

where C and R are the membrane capacitance and resistance, E_L is the leak reversal potential, g_{ex} and g_{in} are the time-dependent excitatory and inhibitory conductances, E_{ex} and E_{in} are the excitatory and inhibitory reversal potentials, I_{tonic} is a constant current applied to all neurons and I_{inp} is a time-varying input described below. Parameters were sampled from Gaussian distributions as described in Table 1. The excitatory and inhibitory conductances, g_{ex} and g_{in} respectively, obey the following equations:

$$\tau_{ex_i}\frac{dg_{ex_i}}{dt} = -g_{ex_i} + \sum_{j=1}^{N_{res}} W_{i,j}G_{ex_i}\delta(t - t^{(j)} - T_{delay}^{(j)}) \tag{2}$$

$$\tau_{in_i}\frac{dg_{in_i}}{dt} = -g_{in_i} + \sum_{j=1}^{N_{res}} W_{i,j}G_{in_i}\delta(t - t^{(j)} - T_{delay}^{(j)}) \tag{3}$$

where τ_{ex} and τ_{in} are the time constants of the excitatory and inhibitory conductances, and G_{in} and G_{ex} are the change in conductance from incoming spikes to excitatory and inhibitory synapses. V_θ is the spiking threshold, $t^{(j)}$ denotes the time since the last spike of the pre-synaptic neuron j, after which V is set to V_{reset} for a duration equal to τ_{ref}. T_{delay} is the propagation delay of the action potential. The reservoir connectivity is defined as a N_{res} X N_{res} sparse and static connectivity matrix W with a density p_{res} (probability of having a non-zero pairwise connection). The non-zero connections are drawn from a half-normal distribution $f(0, \sigma_{res})$, where $\sigma_{res} = \frac{\gamma_{res}}{\sqrt{N_{res}*p_{res}}}$. All ODEs are solved using a forward Euler method with time-step $\Delta t = 0.05$ ms.
Each reservoir neuron is connected to each of the N_{inp} input units with probability p_{inp}. The external inputs (I_{inp}) (with index inp dropped to alleviate notation) follow:

$$I_{i,k}(t) = \frac{A}{2}(\sin(2\pi f_k t + \phi_k) + 1) * M_{i,k} \tag{4}$$

where $i = 1, ..., N_{res}$ stands for the identity of the post-synaptic unit and $k = 1, ..., N_{inp}$, where N_{inp} represents the total number of inputs. f is the frequency of the sine wave and the initial phase ϕ is drawn from a uniform distribution $U(-\pi, \pi)$. The sine wave is then transformed by adding 1 and dividing by 2 to limit its range to [0,A]. The input is rescaled by the connectivity weight $M_{i,k}$ from input unit k into reservoir unit i. The full input-to-reservoir connectivity matrix M is a N_{res} X N_{inp} sparse and static matrix, with a density of p_{inp}. The non-zero connections of M are drawn from a normal distribution $\mathcal{N}(0,1)$ and A is the amplitude of the input (30 pA by default).
All of the reservoir's excitatory neurons project to the readout units. Their spiking activity r is filtered by a double exponential:

$$\tau_d\frac{dr_j}{dt} = -r_j + h_j \tag{5}$$

$$\tau_r\frac{dh_j}{dt} = -h_j + \frac{1}{\tau_d}\sum_{j=1}^{N}\delta(t - t^{(j)}) \tag{6}$$

	Reservoir	Input (oscillatory networks)
N	1,000	500
R	100 $M\Omega$	100 $M\Omega$
C	200 pF	200 pF
E_L	μ = -60 mV, σ = 1.2 mV	μ = -60 mV, σ = 0.6 mV
V_θ	μ = -50 mV, σ = 0.5 mV	μ = -50 mV, σ = 0.5 mV
V_{reset}	μ = -60 mV, σ = 1.2 mV	μ = -60 mV, σ = 0.6 mV
I_{tonic}	90 pA	90 pA
T_{delay}	μ = 1 ms, σ = 0.02 ms	μ = 1 ms, σ = 0.01 ms
τ_{ref}	μ = 2 ms, σ = 0.04 ms	μ = 2 ms, σ = 0.02 ms
G_{ex}	μ = 20 pS, σ = 0.4 pS	μ = 30 pS, σ = 0.03 pS
G_{in}	μ = 160 pS, σ = 3.2 pS	μ = 140 pS, σ = 1.4 pS
τ_{ex}	μ = 20 ms, σ = 0.4 ms	μ = 20 ms, σ = 0.2 ms
τ_{in}	μ = 20 ms, σ = 0.4 ms	μ = 80 ms, σ = 0.8 ms
E_{ex}	0 mV	0 mV
E_{in}	-80 mV	-80 mV
p_{res}	0.1	1
p_{inp}	0.3	1
γ_{res}	1	1

Table 1. Reservoir parameters.

where $\tau_r = 6$ ms is the synaptic rise time and $\tau_d = 60$ ms is the synaptic decay time. W_{out} is initialized as a N_{out} X $N_{res}^{(ex)}$ null matrix that is modified according to the learning rule described below (see training procedure). N_{out} is the number of readout units and $N_{res}^{(ex)}$ is the number of excitatory neurons in the reservoir.

B. Target functions. Unless otherwise stated, the target functions employed to train the model were generated from white noise with a normal distribution $N(0, 30)$, then low-pass filtered with a cut-off at 6 Hz. To assess network performance, we computed the Pearson correlation between the output of the network and the target function.

B.1. Training procedure.

Recursive Least Square. The W_{out} weight matrix is updated with the recursive least-square algorithm (11, 21), adapted to spiking networks (see (13) for full implementation).

B.2. Oscillatory networks. Oscillatory networks obey the same equations as the reservoir networks. However, the I_{inp} term in Eq.1 is replaced by the following step functions:

$$I^{(ex)} = \begin{cases} 0 & \text{if } t_{stim} > t, \text{ or } t > t_{end}^{ex} \\ AW_{in} & otherwise \end{cases} \qquad [7]$$

$$I^{(in)} = \begin{cases} 0 & \text{if } t_{stim} > t, \text{ or } t > t_{end}^{in} \\ AW_{in} & otherwise \end{cases} \qquad [8]$$

where $t_{stim} = 500$ ms, t_{end}^{ex} denotes the end of the excitatory pulse and t_{end}^{in} (different across oscillatory networks) is the end of the inhibitory pulse, where $t_{end}^{ex} > t_{end}^{in}$. W_{in} is a dense matrix with N_{osc} X N_{inp} elements representing the connections from the tonic inputs to the oscillatory networks, where N_{inp} is the number of oscillatory networks projecting to the reservoir and A = 20 pA.

The oscillatory networks each project to the reservoir with a N_{res} X $(N_{osc} * N_{inp})$ sparse and static connectivity matrix M, where each oscillatory network projects to the reservoir with a density of $p_{inp} = 0.5$. The non-zero connections are drawn from a normal distribution $\mathcal{N}(0, \sigma_{inp})$, where $\sigma_{inp} = \frac{\gamma_{inp}}{\sqrt{p_{inp} N_{res} N_{osc}}}$ and $\gamma_{inp} = 10$ (a.u.) by default.

Where stated in the Results, the reservoir projects back to the oscillatory networks with a $(N_{osc} * N_{inp})$ X N_{res} sparse and static connectivity matrix M', where each reservoir unit projects to the oscillatory networks with a density of $p_{fb} = 0.5$. The non-zero connections are drawn from a normal distribution $\mathcal{N}(0, \sigma_{fb})$, where $\sigma_{fb} = \frac{\gamma_{fb}}{\sqrt{p_{fb} N_{res} N_{osc}}}$.

B.3. Selection of stable networks. As we were interested in regimes where the networks would produce reliable and repeatable oscillations to be used as an input to our model, we considered networks with an inter-trial correlation coefficient (10 trials) of their mean firing-rate greater than 0.95 as stable. A wide range of parameter combinations lead to reliable oscillations, but different random initialisations of networks with the same parameters can lead to drastically different behavior, both in activity type (ansynchronous and synchronous) and inter-trial reliability.

B.4. Jitter accumulation in input phase. While a perfect sinusoidal input such as the one in equation 15 allows for well-controlled simulations, it is unrealistic from a biological standpoint. To address this issue, we added jitter to the input phase of each input unit. This was achieved by converting the static input phase injected into unit k ϕ_k to a random walk $\phi_k(t)$. First, we discretize time into non-overlapping bins of length Δt, such that $t_n = \Delta t * n$. From there, we iteratively define $\phi(t)$ (index k is dropped to alleviate the notation) as:

$$\phi_{t+\Delta t} = \phi_t + \varepsilon_t \Longleftrightarrow \phi_{n+1} = \phi_n + \varepsilon_{n+1} \tag{9}$$

with

$$\phi(0) = \phi_0 \tag{10}$$

$$\varepsilon \sim \mathcal{N}(0, \sigma_\phi^2 \Delta t) \tag{11}$$

from initial value ϕ_0, sampled from a uniform distribution as specified previously. More intuitively, $\phi(t)$ can be constructed as:

$$\phi(0) = \phi_0$$
$$\phi_1 = \phi_0 + \varepsilon_1$$
$$\phi_2 = \phi_1 + \varepsilon_2 = \phi_0 + \varepsilon_1$$
$$...$$
$$\phi_N = \phi_0 + \sum_{n=1}^{N} \varepsilon_n \tag{12}$$

On average, the resulting deviation from the deterministic signal, *i.e.* $E[\phi_N - \phi_0]$, is null. On the other hand, one can calculate its variance:

$$var(\phi_N - \phi_0) = var\left(\phi_0 + \sum_{n=1}^{N} \varepsilon_n - \phi_0\right)$$

$$= var\left(\sum_{n=1}^{N} \varepsilon_n\right)$$

Since all ε_n are i.i.d:

$$\sum_{n=1}^{N} var(\varepsilon_n) = N var(\varepsilon_n)$$

$$= N\sigma_\phi^2 \Delta t$$

$$\Leftrightarrow var(\phi_N - \phi_0) = t\sigma_\phi^2 \tag{13}$$

For ease of comparison, we can express the equivalent standard deviation in degrees (see Fig. S7):

$$\sigma_{deg} = \sqrt{t\sigma_\phi^2} \frac{180}{\pi} \tag{14}$$

B.5. Model for place cells sequence formation. We employed a balanced recurrent network similar to the ones used for all other simulations, with a few key differences. The input consisted of $N_{inp} = 20$ oscillators with periods ranging from 7.5 to 8.5 Hz that densely projected to the reservoir ($p = 1$) and follow:

$$I_{i,k}(t) = \sin(2\pi f_k t + \phi_k) + 1) * M_{i,k} \tag{15}$$

C was set to 100 pF for all neurons and γ_{res} was set to 0.5. We removed the readout unit and connections, and we selected 10 random excitatory cells (N_{place}) as place cells. Those cells had parameters identical to the other reservoir excitatory units, except:

1. We set the resting potential of those cells to the mean of E_L, to avoid higher values that could lead to high spontaneous activity (that in turn can lead to spurious learning).

2. A 600 ms sine wave at 10 Hz with an amplitude of 60 pA was injected in each of the place cells at a given time representing the animal going through its place field.

3. The connections between the input oscillators and the place cells were modified following eq.16.

We modelled the environmental input (10 Hz depolarisation of CA1 place cells) based on a representation of the animal's location that was fully dependent on time. In order to explain phase precession, our model relied on an environmental input of a slightly higher frequency than the background theta oscillation, as suggested in (59).

The learning rule seeks to optimize the connections between the oscillating inputs and the place cells in order to make them fire whenever the right phase configuration is reached (18, 19).

We used a band-pass filter between 4-12 Hz to isolate the theta rhythm in the reservoir. We then used a Hilbert transform to obtain the instantaneous phase of the resulting signal.

Vincent-Lamarre *et al.*

Learning algorithm. We developed a correlation-based learning rule (60) inspired by the results obtained by (61):

$$M_{i,k}(t + \Delta t) = M_{i,k} + \alpha I_{inp_k}(t) \qquad [16]$$

where $i = 1, ..., N_{place}$ and $\alpha = 0.25$. With this rule, the weight update is only applied when a burst occurs in the place cells. A burst is defined as any spike triplets that occur within 50 ms. In experiments, these post-synaptic bursts were associated with Ca^{2+} plateaus in place cells (61) that lead to a large potentiation of synaptic strength with as few as 5 pairings. The connections of M were initialized from a half-normal distribution $f(0, \sigma_{inp})$, where $\sigma_{inp} = 0.1$ and the signal amplitude A was set to 1. M was bound between 0 and $5*\sigma_{inp}$ during training.

C. Audio processing for speech learning. We used the numpy/python audio tools from (62), adapted by (63), to process the audio WAVE file. We used the built-in functions to convert the audio file to a mel-scaled spectrogram and to invert it back to a waveform.

D. Data availability. The custom python script used to generate the main results in this manuscript can be found at https://github.com/lamvin/Oscillation_multiplexing.git.

1. Dean V Buonomano and Wolfgang Maass. State-dependent computations: spatiotemporal processing in cortical networks. *Nature Reviews Neuroscience*, 10(2):113–125, 2009. ISSN 1471-003X.
2. Catalin V. Buhusi and Warren H. Meck. What makes us tick? Functional and neural mechanisms of interval timing. *Nat Rev Neurosci*, 6(10):755–765, October 2005. ISSN 1471-003X. . URL http://dx.doi.org/10.1038/nrn1764.
3. Simon Grondin. Timing and time perception: A review of recent behavioral and neuroscience findings and theoretical directions. *Attention, Perception, & Psychophysics*, 72(3):561–582, April 2010. ISSN 1943-393X. . URL https://doi.org/10.3758/APP.72.3.561.
4. Joseph J Paton and Dean V Buonomano. The Neural Basis of Timing: Distributed Mechanisms for Diverse Functions. *Neuron*, 98(4):687–705, 2018. ISSN 0896-6273.
5. L F Abbott, Brian DePasquale, and Raoul-Martin Memmesheimer. Building functional networks of spiking model neurons. *Nature Neuroscience*, 19:350, February 2016. URL https://doi.org/10.1038/nn.4241.
6. Razvan Pascanu, Tomas Mikolov, and Yoshua Bengio. Understanding the exploding gradient problem. *CoRR, abs/1211.5063*, 2, 2012.
7. Carl van Vreeswijk and Haim Sompolinsky. Chaos in neuronal networks with balanced excitatory and inhibitory activity. *Science*, 274(5293):1724–1726, 1996. ISSN 0036-8075.
8. Henry DI Abarbanel, Daniel R Creveling, and James M Jeanne. Estimation of parameters in nonlinear systems using balanced synchronization. *Physical Review E*, 77(1):016208, 2008.
9. Herbert Jaeger. Adaptive nonlinear system identification with echo state networks. pages 593–600, 2002.
10. Wolfgang Maass, Thomas Natschläger, and Henry Markram. Real-time computing without stable states: A new framework for neural computation based on perturbations. *Neural computation*, 14(11):2531–2560, 2002. ISSN 0899-7667.
11. David Sussillo and L.F. Abbott. Generating Coherent Patterns of Activity from Chaotic Neural Networks. *Neuron*, 63(4):544–557, August 2009. ISSN 0896-6273. . URL http://www.sciencedirect.com/science/article/pii/S0896627309005479.
12. Rodrigo Laje and Dean V Buonomano. Robust timing and motor patterns by taming chaos in recurrent neural networks. *Nat Neurosci*, 16(7):925–933, July 2013. ISSN 1097-6256. URL http://dx.doi.org/10.1038/nn.3405.
13. Wilten Nicola and Claudia Clopath. Supervised learning in spiking neural networks with FORCE training. *Nature Communications*, 8(1):2208, December 2017. ISSN 2041-1723. . URL https://www.nature.com/articles/s41467-017-01827-3.
14. H. Francis Song, Guangyu R. Yang, and Xiao-Jing Wang. Training Excitatory-Inhibitory Recurrent Neural Networks for Cognitive Tasks: A Simple and Flexible Framework. *PLOS Computational Biology*, 12(2):e1004792, February 2016. ISSN 1553-7358. . URL https://journals.plos.org/ploscompbiol/article?id=10.1371/journal.pcbi.1004792.
15. Philippe Vincent-Lamarre, Guillaume Lajoie, and Jean-Philippe Thivierge. Driving reservoir models with oscillations: a solution to the extreme structural sensitivity of chaotic networks. *Journal of computational neuroscience*, 41(3):305–322, 2016. ISSN 0929-5313.
16. Wolfgang Maass, Prashant Joshi, and Eduardo D Sontag. Computational Aspects of Feedback in Neural Circuits. *PLoS Comput Biol*, 3(1):e165, January 2007. . URL http://dx.plos.org/10.1371%2Fjournal.pcbi.0020165.
17. Ila R Fiete, Yoram Burak, and Ted Brookings. What grid cells convey about rat location. *The Journal of Neuroscience*, 28(27):6858–6871, 2008. ISSN 0270-6474.
18. Christopher Miall. The storage of time intervals using oscillating neurons. *Neural Computation*, 1(3):359–371, 1989.
19. Matthew S Matell and Warren H Meck. Cortico-striatal circuits and interval timing: coincidence detection of oscillatory processes. *Cognitive Brain Research*, 21(2):139–170, 2004. ISSN 0926-6410.
20. Alain Destexhe. Conductance-based integrate-and-fire models. *Neural Computation*, 9(3):503–514, 1997. ISSN 0899-7667.
21. Simon Haykin. Adaptive filter theory. *Prentice Hall*, 2:478–481, 2002.
22. E. Marder and R. L. Calabrese. Principles of rhythmic motor pattern generation. *Physiological Reviews*, 76(3):687–717, July 1996. ISSN 0031-9333. . URL https://www.physiology.org/doi/abs/10.1152/physrev.1996.76.3.687.
23. Nicolas Brunel. Dynamics of sparsely connected networks of excitatory and inhibitory spiking neurons. *Journal of computational neuroscience*, 8(3):183–208, 2000. ISSN 0929-5313.
24. Nicolas Brunel and David Hansel. How Noise Affects the Synchronization Properties of Recurrent Networks of Inhibitory Neurons. *Neural Computation*, 18(5):1066–1110, March 2006. ISSN 0899-7667. . URL https://doi.org/10.1162/neco.2006.18.5.1066.
25. Jean-Philippe Thivierge, Rosa Comas, and Andre Longtin. Attractor dynamics in local neuronal networks. *Frontiers in Neural Circuits*, 8, 2014. ISSN 1662-5110. . URL https://www.frontiersin.org/articles/10.3389/fncir.2014.00022/full.
26. György Buzsáki and Andreas Draguhn. Neuronal oscillations in cortical networks. *science*, 304(5679):1926–1929, 2004. ISSN 0036-8075.
27. Vishwa Goudar and Dean V Buonomano. Encoding sensory and motor patterns as time-invariant trajectories in recurrent neural networks. *eLife*, 7:e31134, March 2018. ISSN 2050-084X. . URL https://doi.org/10.7554/eLife.31134.
28. Nicholas F. Hardy, Vishwa Goudar, Juan L. Romero-Sosa, and Dean V. Buonomano. A model of temporal scaling correctly predicts that motor timing improves with speed. *Nature Communications*, 9(1):4732, November 2018. ISSN 2041-1723. . URL https://doi.org/10.1038/s41467-018-07161-6.
29. Christopher D Harvey, Philip Coen, and David W Tank. Choice-specific sequences in parietal cortex during a virtual-navigation decision task. *Nature*, 484(7392):62–68, April 2012. ISSN 0028-0836. . URL http://www.ncbi.nlm.nih.gov/pmc/articles/PMC3321074/.
30. Gustavo BM Mello, Sofia Soares, and Joseph J Paton. A scalable population code for time in the striatum. *Current Biology*, 25(9):1113–1122, 2015. ISSN 0960-9822.
31. Konstantin I. Bakhurin, Vishwa Goudar, Justin L. Shobe, Leslie D. Claar, Dean V. Buonomano, and Sotiris C. Masmanidis. Differential Encoding of Time by Prefrontal and Striatal Network Dynamics. *The Journal of Neuroscience*, 37(4):854, January 2017. . URL http://www.jneurosci.org/content/37/4/854.abstract.
32. David J. Foster and Matthew A. Wilson. Hippocampal theta sequences. *Hippocampus*, 17(11):1093–1099, 2007. ISSN 1098-1063. . URL https://onlinelibrary.wiley.com/doi/abs/10.1002/hipo.20345.
33. John O'Keefe. Place units in the hippocampus of the freely moving rat. *Experimental Neurology*, 51(1):78–109, January 1976. ISSN 00144886. . URL https://linkinghub.elsevier.com/retrieve/pii/0014488676900558.
34. George Dragoi, Daniel Carpi, Michael Recce, Jozsef Csicsvari, and György Buzsáki. Interactions between Hippocampus and Medial Septum during Sharp Waves and Theta Oscillation in the Behaving Rat. *Journal of Neuroscience*, 19(14):6191–6199, July 1999. ISSN 0270-6474, 1529-2401. . URL https://www.jneurosci.org/content/19/14/6191.
35. Roger D Traub, Richard Miles, and Robert K S Wong. Model of the origin of rhythmic population oscillations in the hippocampal slice. *Science*, 243(4896):1319–1325, 1989.
36. Romain Goutagny, Jesse Jackson, and Sylvain Williams. Self-generated theta oscillations in the hippocampus. *Nat Neurosci*, 12(12):1491–1493, December 2009. ISSN 1097-6256. . URL http://dx.doi.org/10.1038/nn.2440.
37. Sean M. Montgomery, Martha I. Betancur, and György Buzsáki. Behavior-Dependent Coordination of Multiple Theta Dipoles in the Hippocampus. *Journal of Neuroscience*, 29(5):1381–1394, February 2009. ISSN 0270-6474, 1529-2401. . URL https://www.jneurosci.org/content/29/5/1381.

38. Loren M Frank, Emery N Brown, and Matthew Wilson. Trajectory Encoding in the Hippocampus and Entorhinal Cortex. *Neuron*, 27(1):169–178, July 2000. ISSN 0896-6273. . URL http://www.sciencedirect.com/science/article/pii/S0896627300000180.

39. John O'Keefe and Michael L Recce. Phase relationship between hippocampal place units and the EEG theta rhythm. *Hippocampus*, 3(3):317–330, 1993. ISSN 1098-1063.

40. Albert K. Lee and Matthew A. Wilson. Memory of Sequential Experience in the Hippocampus during Slow Wave Sleep. *Neuron*, 36(6):1183–1194, December 2002. ISSN 0896-6273. . URL http://www.sciencedirect.com/science/article/pii/S0896627302010966.

41. David J. Foster and Matthew A. Wilson. Reverse replay of behavioural sequences in hippocampal place cells during the awake state. *Nature*, 440(7084):680, March 2006. ISSN 1476-4687. . URL https://www.nature.com/articles/nature04587.

42. Alessandro Ingrosso and L. F. Abbott. Training dynamically balanced excitatory-inhibitory networks. *PLOS ONE*, 14(8):e0220547, August 2019. ISSN 1932-6203. . URL https://journals.plos.org/plosone/article?id=10.1371/journal.pone.0220547.

43. Rafael Yuste, Jason N MacLean, Jeffrey Smith, and Anders Lansner. The cortex as a central pattern generator. *Nature Reviews Neuroscience*, 6(6):477–483, 2005. ISSN 1471-003X.

44. Xiao-Jing Wang. Neurophysiological and Computational Principles of Cortical Rhythms in Cognition. *Physiological Reviews*, 90(3):1195–1268, July 2010. ISSN 0031-9333, 1522-1210. . URL http://www.physiology.org/doi/10.1152/physrev.00035.2008.

45. Eve Marder and Dirk Bucher. Central pattern generators and the control of rhythmic movements. *Current Biology*, 11(23):R986–R996, November 2001. ISSN 0960-9822. . URL http://www.sciencedirect.com/science/article/pii/S0960982201005814.

46. Uri Rokni and Haim Sompolinsky. How the Brain Generates Movement. *Neural Computation*, 24(2):289–331, October 2011. ISSN 0899-7667. . URL https://doi.org/10.1162/NECO_a_00223.

47. Mark M. Churchland, John P. Cunningham, Matthew T. Kaufman, Justin D. Foster, Paul Nuyujukian, Stephen I. Ryu, and Krishna V. Shenoy. Neural population dynamics during reaching. *Nature*, 487(7405):51–56, July 2012. ISSN 0028-0836. . URL http://dx.doi.org/10.1038/nature11129.

48. Xiao-Jing Wang. Synaptic reverberation underlying mnemonic persistent activity. *Trends in Neurosciences*, 24(8):455–463, July 2016. ISSN 0166-2236. . URL http://dx.doi.org/10.1016/S0166-2236(00)01868-3.

49. Edvard I. Moser, Emilio Kropff, and May-Britt Moser. Place Cells, Grid Cells, and the Brain's Spatial Representation System. *Annual Review of Neuroscience*, 31(1):69–89, July 2008. ISSN 0147-006X, 1545-4126. . URL http://www.annualreviews.org/doi/10.1146/annurev.neuro.31.061307.090723.

50. Neil Burgess, Caswell Barry, and John O'Keefe. An oscillatory interference model of grid cell firing. *Hippocampus*, 17(9):801–812, 2007. ISSN 1098-1063. . URL https://onlinelibrary.wiley.com/doi/abs/10.1002/hipo.20327.

51. Wilten Nicola and Claudia Clopath. A diversity of interneurons and Hebbian plasticity facilitate rapid compressible learning in the hippocampus. *Nature Neuroscience*, 22(7):1168, July 2019. ISSN 1546-1726. . URL https://www.nature.com/articles/s41593-019-0415-2.

52. Claudio Gallicchio, Alessio Micheli, and Luca Pedrelli. Deep reservoir computing: A critical experimental analysis. *Neurocomputing*, 268:87–99, December 2017. ISSN 09252312. . URL https://linkinghub.elsevier.com/retrieve/pii/S0925231217307567.

53. Robert Schmidt, Kamran Diba, Christian Leibold, Dietmar Schmitz, György Buzsáki, and Richard Kempter. Single-Trial Phase Precession in the Hippocampus. *Journal of Neuroscience*, 29(42):13232–13241, October 2009. ISSN 0270-6474, 1529-2401. . URL https://www.jneurosci.org/content/29/42/13232.

54. David F. Conant, Kristofer E. Bouchard, Matthew K. Leonard, and Edward F. Chang. Human Sensorimotor Cortex Control of Directly Measured Vocal Tract Movements during Vowel Production. *Journal of Neuroscience*, 38(12):2955–2966, March 2018. ISSN 0270-6474, 1529-2401. . URL https://www.jneurosci.org/content/38/12/2955.

55. Gopala K. Anumanchipalli, Josh Chartier, and Edward F. Chang. Speech synthesis from neural decoding of spoken sentences. *Nature*, 568(7753):493, April 2019. ISSN 1476-4687. . URL https://www.nature.com/articles/s41586-019-1119-1.

56. Hojjat Salehinejad, Sharan Sankar, Joseph Barfett, Errol Colak, and Shahrokh Valaee. Recent Advances in Recurrent Neural Networks. *arXiv:1801.01078 [cs]*, December 2017. URL http://arxiv.org/abs/1801.01078. arXiv: 1801.01078.

57. Gouhei Tanaka, Toshiyuki Yamane, Jean Benoit Héroux, Ryosho Nakane, Naoki Kanazawa, Seiji Takeda, Hidetoshi Numata, Daiju Nakano, and Akira Hirose. Recent Advances in Physical Reservoir Computing: A Review. *arXiv preprint arXiv:1808.04962*, 2018.

58. Michele Folgheraiter, Amina Keldibek, Bauyrzhan Aubakir, Giuseppina Gini, Alessio Mauro Franchi, and Matteo Bana. A neuromorphic control architecture for a biped robot. *Robotics and Autonomous Systems*, page S0921889017301793, July 2019. ISSN 09218890. . URL https://linkinghub.elsevier.com/retrieve/pii/S0921889017301793.

59. Máté Lengyel, Zoltán Szatmáry, and Péter Érdi. Dynamically detuned oscillations account for the coupled rate and temporal code of place cell firing. *Hippocampus*, 13(6):700–714, 2003. ISSN 1098-1063. . URL https://onlinelibrary.wiley.com/doi/abs/10.1002/hipo.10116.

60. Richard Kempter, Wulfram Gerstner, and J. Leo van Hemmen. Hebbian learning and spiking neurons. *Physical Review E*, 59(4):4498–4514, April 1999. ISSN 1063-651X, 1095-3787. . URL https://link.aps.org/doi/10.1103/PhysRevE.59.4498.

61. Katie C. Bittner, Aaron D. Milstein, Christine Grienberger, Sandro Romani, and Jeffrey C. Magee. Behavioral time scale synaptic plasticity underlies CA1 place fields. *Science*, 357(6355):1033–1036, September 2017. ISSN 0036-8075, 1095-9203. . URL https://science.sciencemag.org/content/357/6355/1033.

62. Kyle Kastner. Audio tools for numpy/python., March 2019. URL https://gist.github.com/kastnerkyle/179d6e9a88202ab0a2fe.

63. Tim Sainburg. Spectrograms, MFCCs, and Inversion in Python, July 2018. URL https://timsainburg.com/python-mel-compression-inversion.html.

64. Johnatan Aljadeff, David Renfrew, Marina Vegué, and Tatyana O. Sharpee. Low-dimensional dynamics of structured random networks. *Physical Review E*, 93(2):022302, February 2016. . URL https://link.aps.org/doi/10.1103/PhysRevE.93.022302.
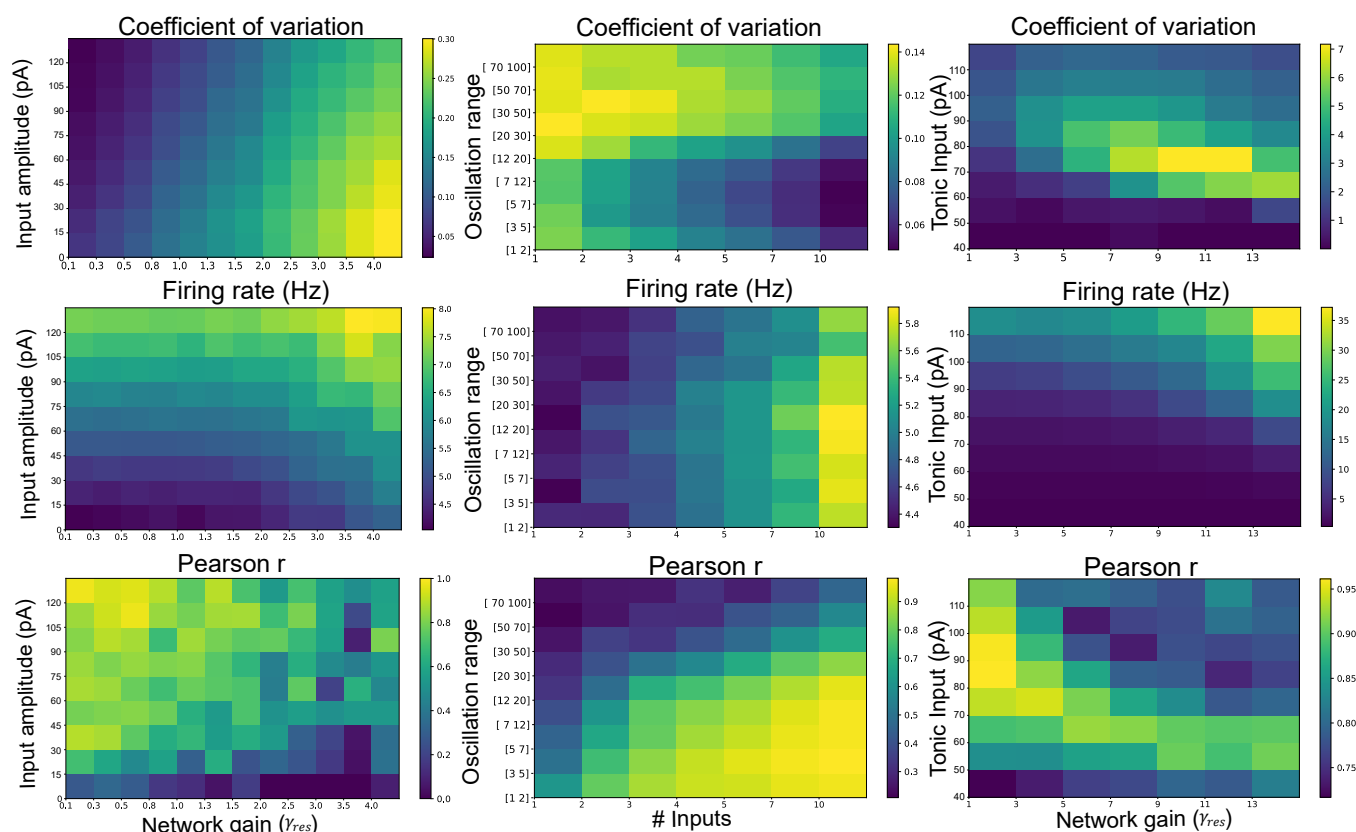
Supporting Information

Fig. S1. Parameter exploration for training a reservoir network. The top row shows the average CV, the middle row shows the average firing rate, and the bottom row shows the average correlation between the output of the network and the target output. *Input amplitude* is the strength of the the input projecting to the reservoir's units. *Network gain* is the strength of the recurrent connections between the reservoir's units. *Oscillation range* is the range from which each input unit's sine wave period is randomly drawn. *# Inputs* is the number of different input units projecting to the reservoir. *Tonic input* is the strength of the constant current injected to each of the reservoir's units.

Fig. S1 shows the impact of different network parameters on the model's performance. We used three measures of the network's activity and performance: 1- The average coefficient of variation (CV) between trials for each cell. A low CV shows that the ratio of across-trial variability is low relative to the mean firing rate. 2- The average firing rate across all trials. 3- The average correlation between the output of the network and the target function after training.
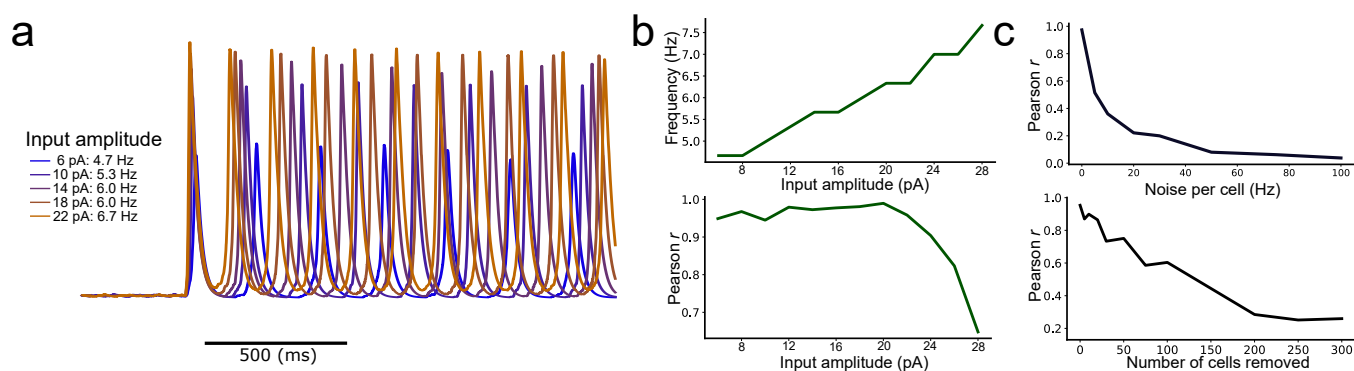
Fig. 2. Autonomous production of repeatable periodic activity. **a** Network activity as a function of the strength of the external drive. The frequency scales with the strength of the tonic input. **b** Top: Average frequency of the network's activity as a function of the external drive. Bottom: Pearson correlation between multiple trials as a function of the amplitude of the external drive. **c** Pearson correlation between multiple trials for a given network as a function of the rate of noisy synaptic input per neuron (top) and as a function of the proportion of clamped neurons (bottom).

For a given network, it is possible to modulate the frequency of its activity by tuning the gain of the tonic input it receives. Stronger external inputs lead to a faster period, up to a limit after which the stability of the activity degrades (Fig.2a,b). The activity of oscillatory networks remains stable in the presence of noise, as the network's cells received trains of synaptic inputs drawn from a Poisson distribution with increasing frequencies and the networks were all robust to clamping a subset of their neurons to their resting potential for the duration of the simulation (Fig.2c).
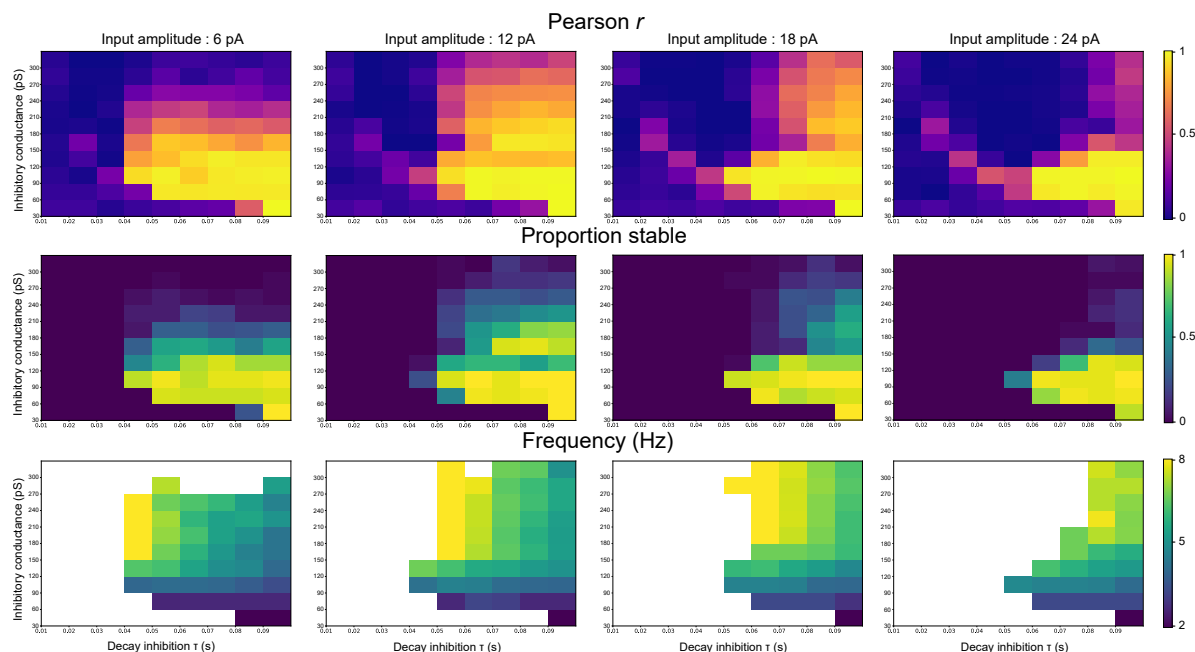
Vincent-Lamarre *et al.*

Fig. 3. Parameter exploration of the network's synchronous activity (inhibition conductance and kinetics). Each column represents a different strength of the external input step, and each heatmap shows different combinations of the conductance and synaptic time-constant of inhibitory inputs. The top row shows the average Pearson correlation between the output and the target function for 5 trials for each of the 50 random network initializations tested per condition. The middle row shows which proportion of the networks are considered as stable. The bottom row shows the average frequency of the periodic activity of the stable networks.

We explored the impact of network parameters on the production of repeatable periodic activity. We were interested in networks that were spontaneously active and that switched to a synchronized regime when driven by a constant tonic input. Starting with networks identical to the reservoir except for its size (500 cells instead of 1000), we tuned the gain and time-scale of inhibitory inputs as well as the gain of the external input and the network sparseness, and monitored the dynamics of the network. We found that all those parameters were crucial in shaping the transition between oscillatory and asynchronous regimes.

To assess to repeatability of network activity, we computed the Pearson correlation of the firing rate fluctuations during each trial with the first trial for every network (Fig.3). Overall, regions of lower inhibition conductance and higher inhibitory synaptic time-constants favour the emergence of repeatable oscillations. The strength of the tonic input also had an impact on the network activity.
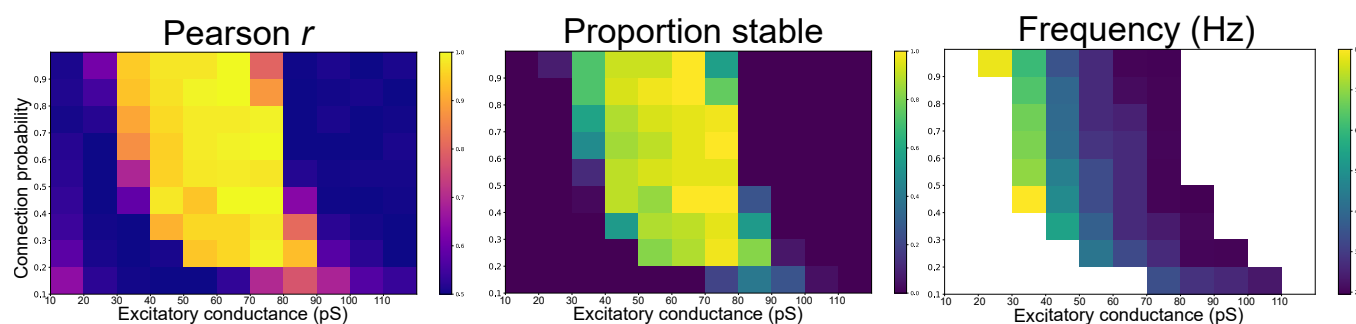
Fig. 4. Parameter exploration of synchronous activity (excitatory conductance and *p*). The sparseness of the reservoir and the conductance of the excitatory connections were systematically varied to observe their impact on the network's regime. *Left*: Pearson correlation between the output and the target function for 5 trials for each of the 50 random network initializations tested per condition. *Middle*: proportion of networks that are considered stable. *Right*: average frequency of the periodic activity of the stable networks.
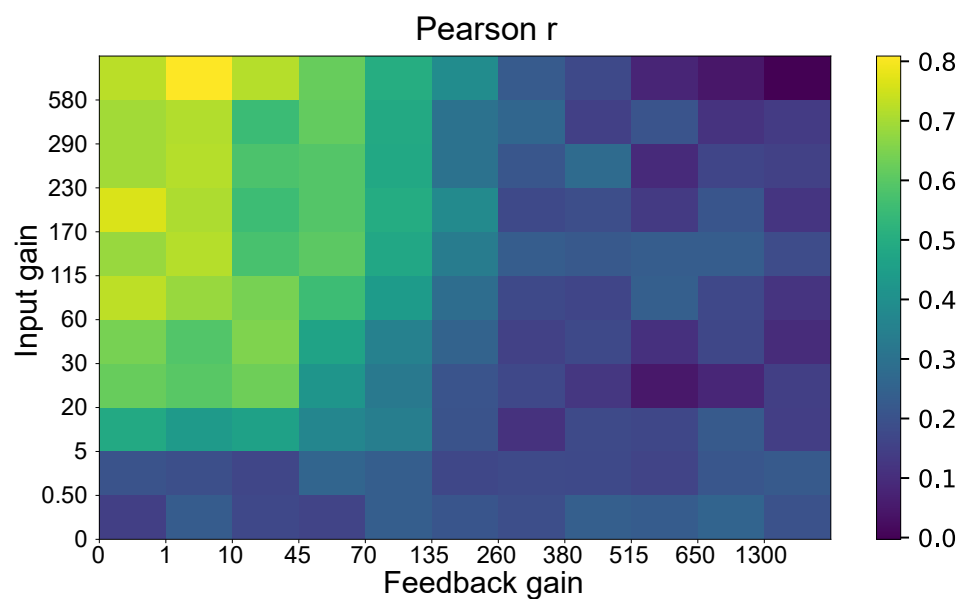
Vincent-Lamarre   *et al.*

Fig. 5. Impact of reservoir feedback to the oscillatory networks. The models can perform well when the gain of the feedback connections from the reservoir to the oscillatory networks are scaled up to a limit. The effect of the feedback gain appears to be independent of the strength of the tonic input of the step function to the oscillatory networks.
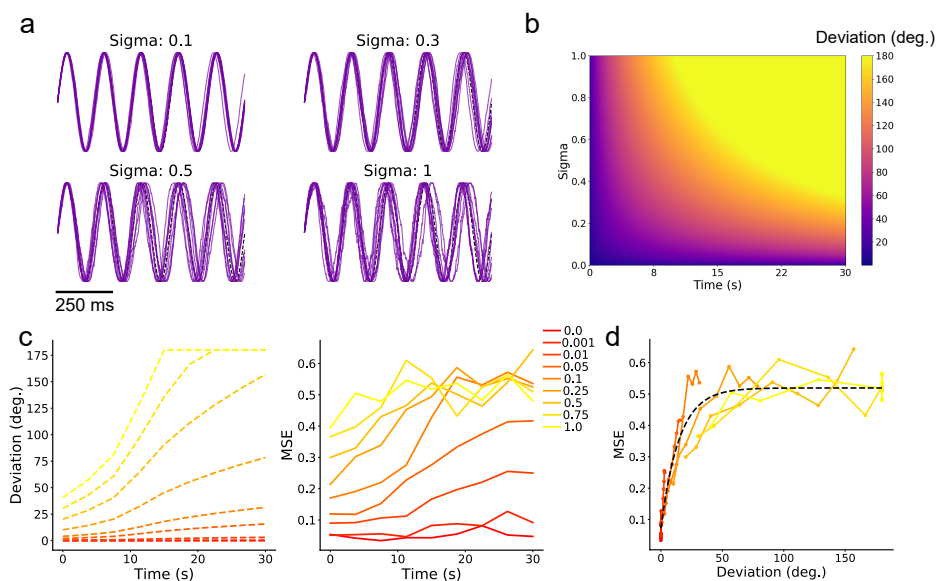
Fig. 6. Network performance with desynchronized inputs. **a** Four simulations of 10 trials each with different σ_ϕ with a random walk process added to the phase of a sine wave. **b** Analytical standard deviation (in degrees) around the expected phase of a deterministic signal as a function of time at different values of σ_ϕ. **c** Left: Analytical estimation of the standard deviation in degrees with the different σ_ϕ used for the network simulation. Right: corresponding MSE between the output and target of the readout unit for the different conditions tested. **d** Relationship between the deviation in degree and the MSE. An exponential function was fit to the data (R^2=0.92).

We simulated a random-walk process $\phi(t)$ (see Methods) with a standard deviation σ_ϕ that we added to the phase of an oscillator (Fig.6a). Because the noise of the random walk comes from a Gaussian process with mean 0, the expected deviation from the base sinusoid is null at all time steps, but its standard deviation at time t is equal to $\sqrt{t * \sigma_{phi}}$ (Fig.6b).

We then trained our model with different σ_{phi} values for different durations. Fig.6c shows the expected standard deviation in degrees for the σ_ϕ used in our simulation, and well as the corresponding error between the output and target functions. Our results show that error accumulates exponentially ($R^2 = 0.92$, Fig.6d). This means that networks can tolerate a deviation of up to 50 degrees from the original sine wave before reaching random performance (defined as the plateau in MSE of the output in Fig.6c,d).
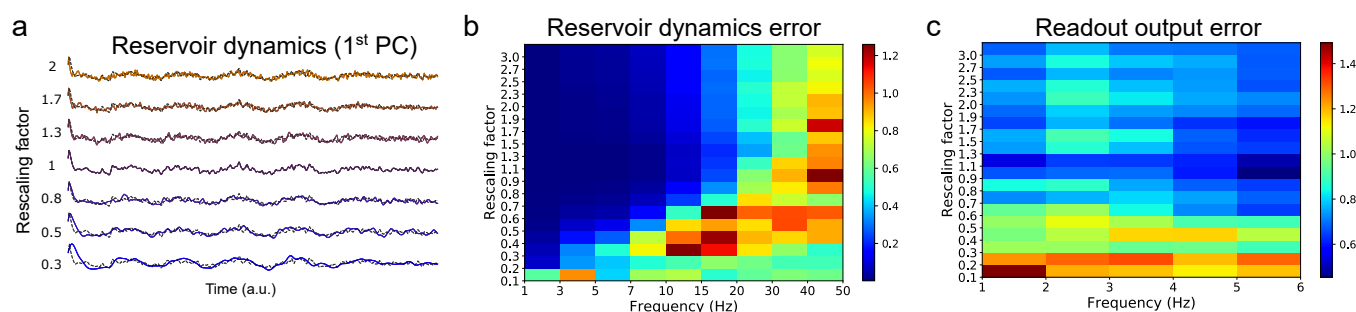
Fig. 7. Network dynamics and performance with temporal rescaling. **a** Activity of the reservoir projected on the first principal component for different rescaling factors. The black dashed line represents the activity without rescaling. The traces displayed have been scaled back to the original velocity. **b** Normalised error of the first principal component of the reservoir's activity for different rescaling factors and frequency bands. **c** Normalised error of the network's output (MSE between the output and the target divided by the total variance of the target function) for different rescaling factors and frequency bands.

We examined whether the qualitative differences in performance slopes between faster and slower rescaling is reflected in the reservoir's activity. We first obtained the projection of the reservoir's activity on the first principal component (accounting for most of the variance of the reservoir, which is typical for this type of network (64)). We then scaled back the activity of the first principal component to the original scaling for all the rescaling factors tested (Fig.7a). This allowed us to compare the features of the reservoir's activity at the original scale. We used a Fourier analysis to obtain a representation of the reservoir's activity for all rescaling factors at different frequencies (Fig.7b). For each rescaling and each frequency band tested, we computed an "error" value defined as the mean squared difference between the reservoir's activity scaled back to the original velocity and the activity of the reservoir on the original scaling at a given frequency. Each error value was then normalized by the square of the frequency band for the target (thus making comparisons of error across frequencies possible).

This analysis revealed that the higher frequencies of the network activity deteriorated faster than the lower frequencies. The lower frequencies were well-preserved for inputs that were slowed down, but were progressively lost for faster rescalings. This explains why the performance reached a plateau (in the absence of input noise) for longer rescaling. We used the same normalization process to examine the output performance across different velocities (Fig.7c). We computed the error for each frequency until 6 Hz given that the target function was generated by applying a low-pass filter on white noise at this cut-off. All frequencies degraded evenly for faster velocities. However, unlike the reservoir's activity, the higher frequencies appeared to be more preserved for the output, whereas the lower frequencies (<4Hz) were more degraded. These results show that rescaling the input frequencies lead to complex modifications of the reservoir dynamics, and highlight a non-trivial relationship between the input and output of the model.